Progress In Electromagnetics Research, PIER 86, 1–18, 2008

AN IMPULSE-RADIO-BASED ULTRAWIDEBAND RF FRONT-END MODULE WITH A NEW MULTILAYERED MICROWAVE SAMPLER

T.-G. Ma, C.-J. Wu, and C.-F. Chou

Department of Electrical Engineering
National Taiwan University of Science and Technology
43, Keelung Rd. Sec. 4, Taipei 10607, Taiwan, R.O.C.

Abstract—In this paper we develop a new impulse-radio-based RF front-end module for ultrawideband communications. The proposed transceiving module is designed based a novel compact microwave sampler. The microwave sampler consists of a multilayered magic-T and a balanced sampling bridge. By utilizing a wideband microstrip-to-slotline Marchand balun, the newly proposed magic-T features an improved bandwidth of 94.2%. The design concept, circuit topology, and experimental results of the magic-T and microwave sampler are investigated in the first half of this paper. By utilizing the equivalent time sampling theory, in the second half of this paper we investigate an impulse-radio-based ultrawideband transceiving front-end module. Two transmission data rates, 90 and 270 Kbps, are demonstrated with various bit patterns. The experimental results reveal that the transceiving module has a coverage range up to 4.5 m. The circuit configuration, modulation scheme, and system performance of the front-end module are discussed thoroughly. The tradeoff for increasing the data rate is discussed at the end of this paper as well.

1. INTRODUCTION

Since the regulations by Federal Communication Committee (FCC) in United States in 2002, the ultrawideband (UWB) system has experienced a blooming growth in both industrial and academic fields. By dividing the allocated spectrum into sub-frequency bands, the ultrawideband system for wireless personal area networks (WPANs) provides high speed data transmission rate up to hundreds of Mbps in a 10-meter area. Meanwhile, the impulse-radio-based ultrawideband system, which transmits and receives baseband pulses without a

carrier, is still very attractive to a variety of applications owing to its low circuit complexity, no need of mixing circuit, undetectable power spectral density, and high immunity against multi-path interference. In an impulse-radio-based ultrawideband system, subnanosecond impulses are used not only for transmitting the data streams but also for downsampling the received pulses in the receiver. It features various advantages over conventional communication radios [1–3]. The aim of this paper is to investigate a new impulse-radio-based ultrawideband RF front-end module for in-vehicle communication. A prototype module is realized with the help of a new multilayered magic-T [4]. The magic-T features a wide bandwidth and compact size. The design concept, methodology and simulated and experimental results will be discussed in Section 2 of this paper.

The magic-T in Section 2 was optimized for microwave sampler application. A microwave sampler is an essential component in an impulse-radio-based ultrawideband communication system. Essentially, a microwave sampler can be viewed as a down-conversion mixer in time domain [5]. Dissimilar to a conventional mixer, nevertheless, a microwave sampler applies subnanosecond pulses instead of continuous wave at its local oscillator (LO) port. It has the ability to sample a periodical RF signal at shot instants. By utilizing the equivalent time sampling (ETS) theorem [6], a down-scaled version of the periodical signal at the RF port can be reproduced at the intermediate frequency (IF) port with a very low repetition frequency. In this sense, a microwave sampler is simply a mixer which is capable of down-converting an arbitrary periodical RF signal with a great amount of harmonics [5]. It replaces the functionality of the down-converter mixing circuit in a conventional communication system. With the microwave sampler, the mixer, voltage-controlled oscillator and the phase-lock loop can be removed without causing damage. It greatly reduces the complexity of the proposed module. Several literatures have been devoted themselves to investigating the microwave sampling circuits [7–9]. Most of the designs are developed with balanced diode configurations and magic-Ts. The balanced structures are especially suitable for microwave sampler due to their inherently excellent isolation properties. It can be applied to mixer [10], phase detector [11], frequency discriminator [12], etc. as well. The requirements of a microwave sampler generally include compact size, low conversion loss, and high linearity. In Section 3, a new microwave sampler will be developed by utilizing a balance sampling bridge and the magic-T in Section 2. This new design features a compact size of 25 by 28 by 1.6 mm^3. It is investigated carefully in time domain with the help of a high-speed digital oscilloscope.

The circuit configuration of the proposed impulse-radio-based ultrawideband RF front-end module is discussed in Section 4. The transmitting module consists of a low-frequency excitation circuit, a modulator, an impulse generator, and a power amplifier. The modulator is realized by a single-pole-double-throw (SPDT) switch. The receiving module, on the other hand, is composed of a microwave sampler, a template pulse generator along with low-frequency excitation circuit and an active lowpass filter. The performance of the transceiving module is demonstrated and discussed by both transmission links over coaxial cable and air interface. This paper is concluded with a brief summary in Section 5.

2. DESIGN OF THE NEW MAGIC-T

The magic-T, or the 180° hybrid coupler, is known as one of the core components in various microwave circuits [13–20]. Conventional magic-Ts are commonly designed with double-sided printed circuit broads by utilizing quarter-wavelength lines in either microstrip form [13], stripline form [14], microstrip/slotline hybrid form [15, 16], coplanar waveguide (CPW)/slotline hybrid form [17], or waveguide form [18]. The sizes of these designs, nonetheless, are inevitably large due to the existence of multiple quarter-wavelength lines. To tackle this problem, an aperture coupled magic-T is proposed in [19] on a three-layered circuit board with a high dielectric constant ($\varepsilon_r = 10.2$). The operation bandwidth, however, is limited to several percentages. A multilayered magic-T with a significantly improved bandwidth of 78% has also been demonstrated on a low-loss Rogers RT-5880 substrate ($\varepsilon_r = 2.2$) [20].

To design a compact multilayered magic-T with an even wider bandwidth, recently we discussed a new aperture coupled microstrip magic-T with a wideband microstrip-to-slotline Marchand balun [4]. The proposed design was fabricated on a low cost FR4 epoxy substrate to fulfill the cost reduction requirement. The circuit layout of the proposed magic-T is illustrated in Fig. 1(a). The proposed design consists of three metal layers. On the top layer (Layer 1), the microstrip line connected to port 1 is terminated with an open-circuited radial stub. A chip resistor is connected to the open end of the stub and provides the necessary current return path and resistive loading for the pulse generator attached to port 1. The resistor also minimizes the multi-reflections between the radial open stub and the cross-junction of the microstrip line and slotline. A microstrip T-junction along with a quarter-wavelength impedance transformer is printed on the bottom layer (Layer 3) of the magic-T. The layer in-between (Layer 2) is a common ground plane with a coupling slotline etched on it. A

short-circuited radial stub is etched at one end of the coupling slot. Essentially, the microstrip line on the top layer and the slotline on the common ground plane form a wideband Marchand balun. It plays a key role in further broadening the operation bandwidth of the magic-T.

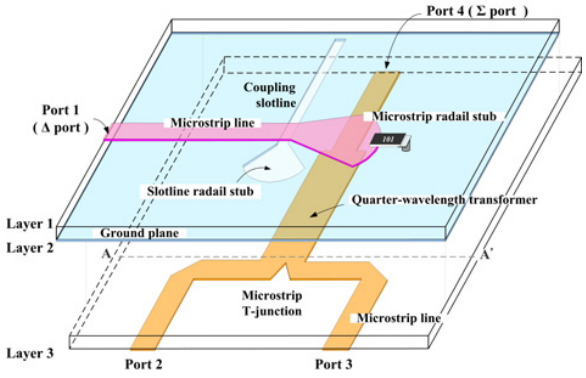

(a)

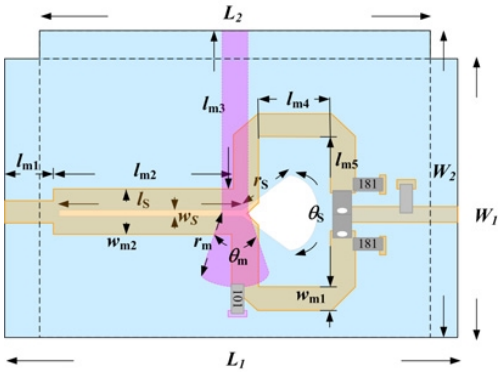

(b)

Figure 1. Configuration of the proposed (a) magic-T and (b) microwave sampler.

In the magic-T, the port 1 serves as the difference (Δ) port whereas the port 4 acts as the sum (Σ) port. The ports 2 and 3, on the other hand, are the output ports of the circuit. Shown in Figs. 2(a) and (b) are the electric field distributions along the cross section A-A' of the magic-T as the difference and sum ports are excited, respectively. The operation principles have been well explained in [4] and will not be repeated here for brevity. The proposed magic-T was designed using EM simulator Ansoft HFSS 10.1, and was

fabricated on a multilayered FR4 epoxy substrate each with a thickness of 0.8 mm. The dielectric constant and loss tangent of the substrate are 4.4 and 0.022, respectively. The optimized dimensions are given as follows: $L_1 = 23\,\text{mm}$, $L_2 = 19\,\text{mm}$, $W_1 = 23\,\text{mm}$, $W_2 = 25\,\text{mm}$, $l_{m1} = 3\,\text{mm}$, $l_{m2} = l_{m5} = 11\,\text{mm}$, $l_{m3} = l_s = 12.5\,\text{mm}$, $l_{m4} = 4.5\,\text{mm}$, $w_{m1} = 1.5\,\text{mm}$, $w_{m2} = 3.2\,\text{mm}$, $w_s = 1\,\text{mm}$, $r_s = 2.62\,\text{mm}$, $r_m = 4.74\,\text{mm}$, $\theta_s = 60°$, and $\theta_m = 45°$. For demonstration purpose in the laboratory, the two layers of FR4 substrates were initially fabricated independently, and the ground planes of substrates were jointed together by adhesive around the peripherals. The ground planes were kept electrically short-circuited to guarantee proper operation. The overall size of the magic-T is 25 by 23 by $1.6\,\text{mm}^3$. The simulated and measured S-parameters are shown in Fig. 3. The measurement was taken by an Agilent E8362B network analyzer. The measurement agrees very well with the simulation. The measured return losses at all ports are better than 9.5 dB (i.e., VSWR < 2) from 1.5 to 7 GHz. The measured 3-dB insertion loss bandwidth between ports 2 and 1, i.e., S_{12}, is 4.41 GHz. It corresponds to a fractional bandwidth of 94.2%. The minimum insertion loss observed is 5 dB, which is 2 dB apart from the ideal 3-dB power splitting principle. The slightly higher insertion loss in the proposed design can be attributed to the lossy nature of the FR4 substrate used. It can be further improved by utilizing a low-loss substrate, say, Rogers RO4003C. The overall cost, nevertheless, will rise accordingly. It is an apparent trade-off between

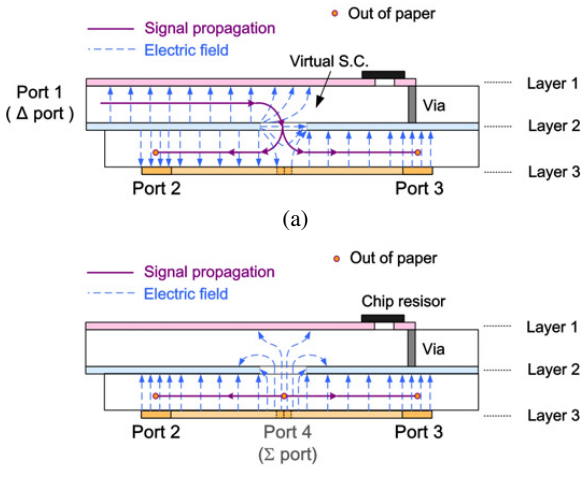

Figure 2. Electric field distributions of the magic-T along the cross section A-A'. (a) Difference port excitation. (b) Sum port excitation.

circuit performance and cost. On the other hand, the transmission coefficient at the sum port, i.e., S_{42} or S_{43}, reveals a better insertion loss of 3.7 dB. It deviates from the ideal value by only 0.7 dB. It also features a wider 3-dB insertion loss bandwidth from 0.5 to 8 GHz. The isolation between the sum and difference ports is better than 35 dB over the frequency range of concern. Shown in Fig. 3(d) is the phase difference between the two output ports as the sum and difference ports are driven alternatively. Well-behaved phase response can be observed throughout the whole band.

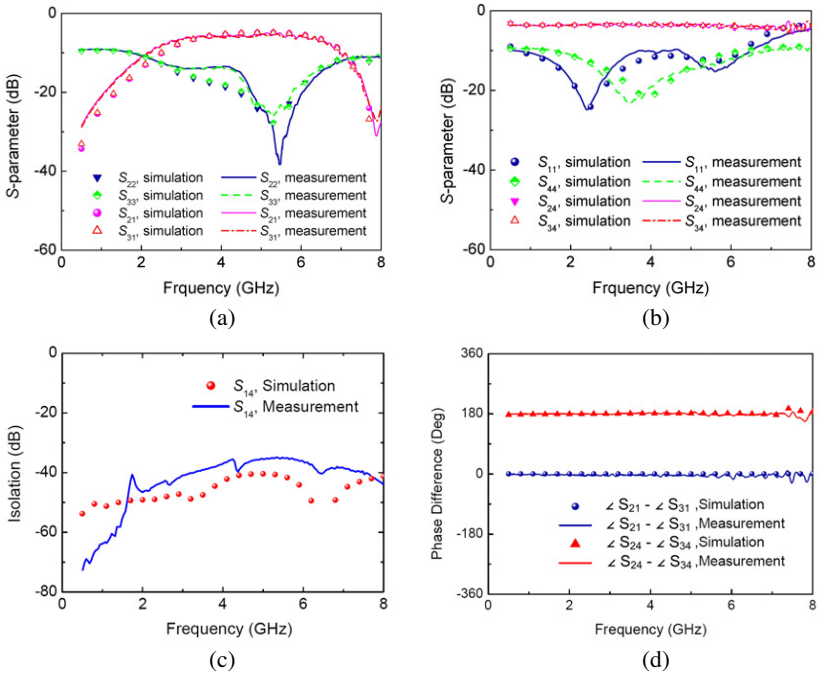

Figure 3. Simulated and measured S-parameters of the proposed magic-T.

3. THE MICROWAVE SAMPLER

By utilizing the proposed magic-T, we demonstrate a multilayered microwave sampler in this section. The configuration of the proposed microwave sampler is shown in Fig. 1(b) along with the geometric parameters. Fig. 4 illustrates the schematic diagram of the microwave sampler together with the pulse generators, sampling bridge, and IF lowpass filter. As shown in the figure, the pulse generator at the LO

port periodically sends strobe signals for sampling the RF waveform. A pair of Schottky diodes with the same polarity is connected to the output ports, i.e., ports 2 and 3, of the magic-T. It forms a balanced sampling bridge. The sampling diode used is a low-barrier, low junction capacitance Schottky diode from M/A-COM® with part number MA4E2054-1141T. The IF signal is extracted in between the diode pair, and is terminated by a shunted RC tank. In practical application, the input impedance of the next stage can serve as the RC loadings.

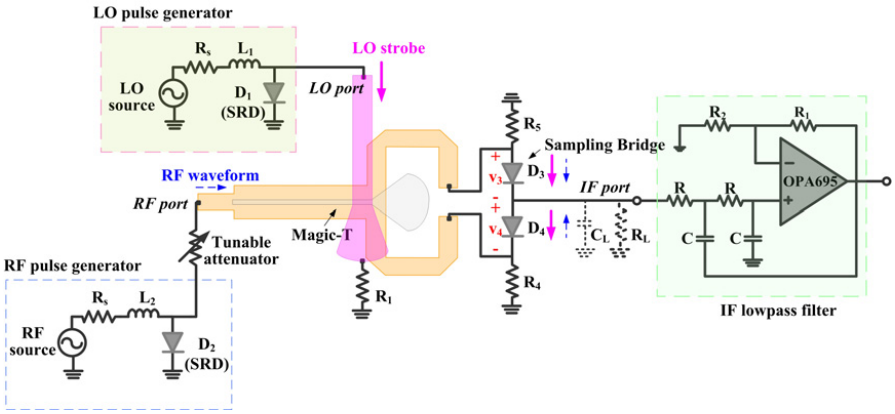

Figure 4. Configuration of the proposed microwave sampler along with the pulse generators and active lowpass filter.

The strobe signals at the sampling bridge can be realized in several ways [21, 22]. In this paper, the strobes are enabled by a shunt-mode pulse generator [22]. The pulse generator consists of a series inductor L_1, a series resistor R_1 and a shunt-to-ground step recovery diode (SRD) D_1. The SRD applied here is a SMMD-0840 diode from the Metelics® Cooperation. The shunt-mode pulse generator provides Gaussian-like impulses at its output. The operating principle has been well explained in the literatures [4, 22] and will not be addressed here for the sake of simplicity. The proposed microwave sampler was also designed on a multilayered FR4 epoxy substrate. The design features a compact size of 25 by 28 by 1.6 mm^3.

To validate the performance of the proposed microwave sampler, the magic-T was first simulated by Ansoft HFSS. The output S-parameters were then imported into Agilent ADS 2006 to complete the simulation. The Agilent ADS is known to have the capability of modeling the nonlinear behavior of the step recovery diode in time domain. A similar shunt-mode pulse generator is applied to the

RF port along with a tunable attenuator for demonstration purpose. The tunable attenuator inserted in-between the pulse generator and the magic-T can provide an adequate attenuation. It mimics the received waveform by the receiving module over air interface. In the measurement, both pulse generators are driven by Agilent vector signal generators E4438C. The operating frequencies of RF and LO signals are 294.9 MHz and 294.4 MHz, respectively. The measured waveforms at various points along the microwave sampler are illustrated in Figs. 5(a)–(d). The simulated results are in reasonable agreement with the measured ones. They are not shown in the figures for the sake of simplicity. Fig. 5(a) shows the measured waveform at the RF port of the microwave sampler. The measurement was taken by an Agilent real-time digital oscilloscope 54855A along with the 1134A probing system. The sampling rate is 5 GSample/s. The RF pulse has a peak voltage of −120 mV and the pulse width is 1 ns. Fig. 5(b) depicts the measured waveforms across the sampling diodes. The waveforms are with equal amplitude but reverse pulse polarity. The Gaussian-like strobe signals are converted into monocycle pulses at the diode

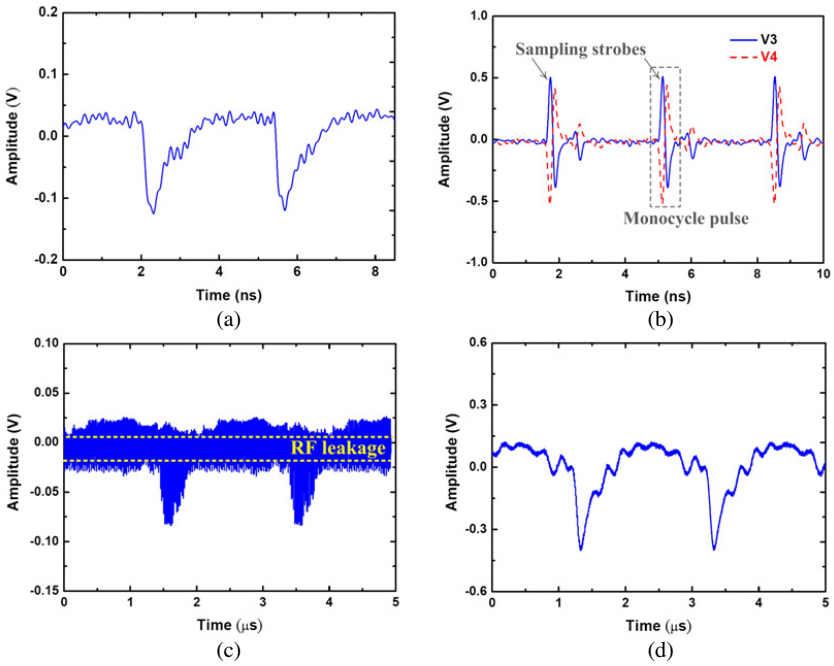

Figure 5. Measured waveforms (a) at the RF port, (b) across the sampling diodes, (c) at the IF port, and (d) at the filter output of the microwave sampler.

junction due to multi-reflections. The monocycle waveform is more preferable since it can force the sampling diode to turn off rapidly and helps improve the sampling accuracy [9]. The pulse width of the sampling strobe is 380 ps, and the voltage difference across the diodes is higher than 1 V. The output waveform at the IF port is shown in Fig. 5(c). The IF signal actually consists of thousands of LO strobes. Each strobe signal was amplitude-modulated by the RF signal at the sampling period. The IF pulse has a peak voltage of −70 mV, which corresponds to a conversion loss of 9.4 dB in a 50-ohm system. The pulse width of the IF signal is 0.5 µs, and the repetition frequency is 500 KHz. Additionally, it is worthwhile to mention that owing to the nonzero reverse-biased junction capacitance of the sampling diode, the RF signals may AC couple to the IF port even when the sampling diodes are turned off. It gives rise to the RF leakage shown in Fig. 5(c). To filter out the high frequency components arisen from both the sampling strobes and RF leakage, we implement an active filter at the output of the microwave sampler, as illustrated in Fig. 4. The operational amplifier used is from TI Corporation with part number OPA695. The cutoff frequency is 8 MHz and the DC gain is 2.2. The filtered-out signal is shown in Fig. 5(d). The peak voltage is −0.4 V and the pulse repetition frequency is also 500 KHz. It is evident that the sampled waveform at the IF port is quite similar to the RF input except that the time scale has been downscaled to the microsecond (µs) order. Finally, it should be emphasized that in theory the RF waveform in the proposed microwave sampler could be an arbitrary periodical signal as long as the difference between the periods of the RF and LO signals is small enough to provide an adequate amount of sampling points.

4. ULTRAWIDEBAND RF FRONT-END MODULE

In this section, an impulse-radio-based ultrawideband transceiving module is demonstrated by implementing the multilayered microwave sampler. The proposed transceiving module aims at implementing in the RF front-end of a variety of ultrawideband systems such as in-vehicle communications, surveillance systems, and etc. The schematic circuit diagrams of the transmitting and receiving modules are shown in Figs. 6(a) and (b), respectively. In the transmitting module, the CITIZEN® crystal oscillator CSX-750FC generates a clock signal with a clock rate of 32.768 MHz and peak-to-peak amplitude of 1.6 V. A TI® frequency multiplier SN65LVDS150 multiplies the clock frequency by a factor of 9. The multiplier is followed by a differential line driver SN65LVDT2DBVR to convert the differential signal at the output of

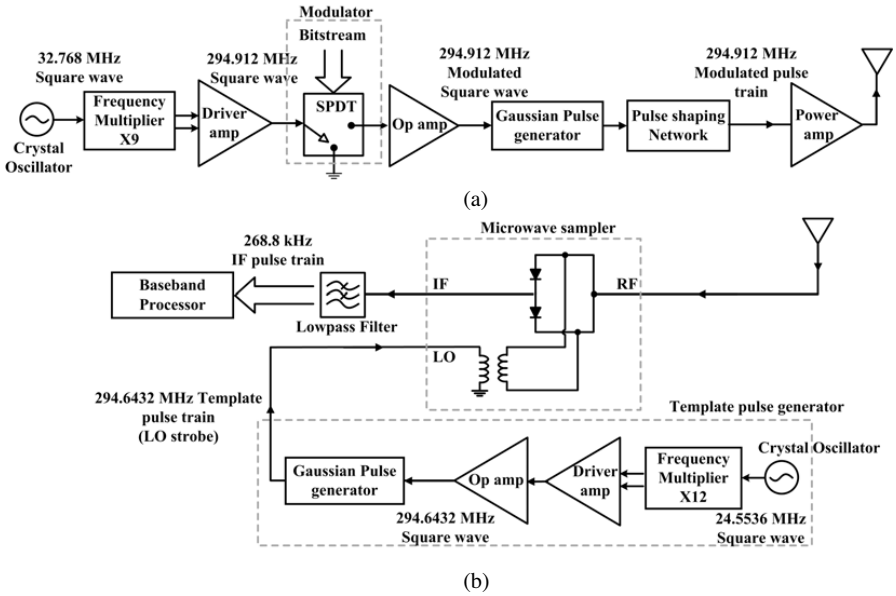

Figure 6. Schematic diagram of the proposed impulse-radio-based ultrawideband RF front-end. (a) Transmitting module. (b) Receiving module.

the multiplier to a single-end one at the input of the modulator. The modulator is implemented by a TI® single-pole-double-throw (SPDT) switch with part number TS5A3157. In the circuit implementation, we choose binary on-off keying due to its low circuit complexity. The baseband bitstream amplitude-modulates the 294.912-MHz square wave by controlling the modulator output. It allows the square wave to pass through when the bit is high. On the other hand, as the bit is low the modulator output is shorted to ground. To properly trigger the shunted-mode pulse generator, a feedback amplifier is attached to the output of the modulator to magnify the modulated square wave. The output signal has a peak-to-peak voltage of 5 V. Fig. 7 shows the circuit configuration of the shunt-mode pulse generator along with a pulse shaping network. The pulse shaper consists of three resistive-loaded shunt stubs and two series lumped capacitors C_1 and C_2. In addition to serve as a resistive loading for eliminating the late-time ringing, the shaping network also acts as a second-order differentiation operator. By the differentiation operation, the pulse shaper can reallocate the spectrum of the incoming Gaussian pulse, which is known to have a large number of low-frequency components, to a higher frequency

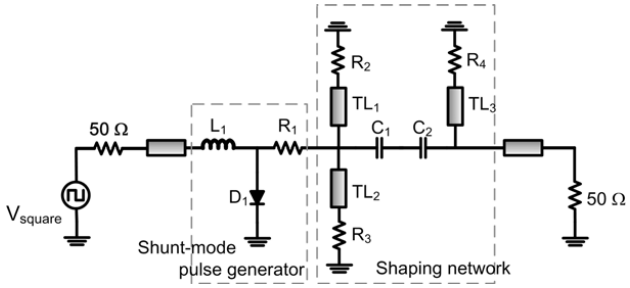

Figure 7. Configuration of the pulse generator and shaping network in the transmitting module.

range. It therefore facilitates the transmission over air interface using an ultrawideband antenna with acceptable size. The pulse generator is also optimized by the software Agilent ADS 2006. The elements are given by $L_1 = 6.8\,\text{nH}$, $R_1 = 33\,\Omega$, $R_2 = R_3 = R_4 = 12\,\Omega$, $C_1 = 0.5\,\text{pF}$, and $C_2 = 1\,\text{pF}$. All the stubs are 1-mm-long 50-ohm microstrip lines. The pulse generating network is followed by a power amplifier, and the output modulated pulse train is transmitted to free space via an ultrawideband antenna. Fig. 8(a) illustrates the antenna used for transmitting and receiving the modulated pulse train. The antenna is a planar monopole antenna developed in our laboratory [23, 24]. The bottom part of the radiator is described by an elliptical profile. It helps improve the impedance matching over a wide bandwidth. The pentagon on the upper part of the antenna may further lengthen the electrical current path and hence lower down the lowest operating frequency. The overall antenna size including the finite size ground plane is $60 \times 60\,\text{mm}^2$. The geometric parameters are $L_a = 22.4\,\text{mm}$, $L_b = 12\,\text{mm}$, $r_1 = 22\,\text{mm}$, $r_2 = 20\,\text{mm}$, and $L_{GND} = 20\,\text{mm}$. The simulated and measured return losses are shown in Fig. 8(b). The agreement between the results is very well. The operating bandwidth with return loss better than 10 dB is from 2 to more than 11 GHz. The simulated and measured radiation patterns at 4 GHz, i.e., the center frequency of the pulse spectrum, are illustrated in Fig. 8(c). For simplicity here only the co-polarized component, E_θ, in the xy-plane is shown. Referring to the figure, the antenna demonstrates quite omnidirectional pattern at the principal plane. The measured antenna peak gain, which occurs at the broadside direction, is 2.7 dBi.

The receiving module consists of a template pulse generator, a microwave sampler, and an active lowpass filter. In Fig. 6(b), the multilayered microwave sampler has been represented by its equivalent circuit model. The template pulse generator has a similar configuration

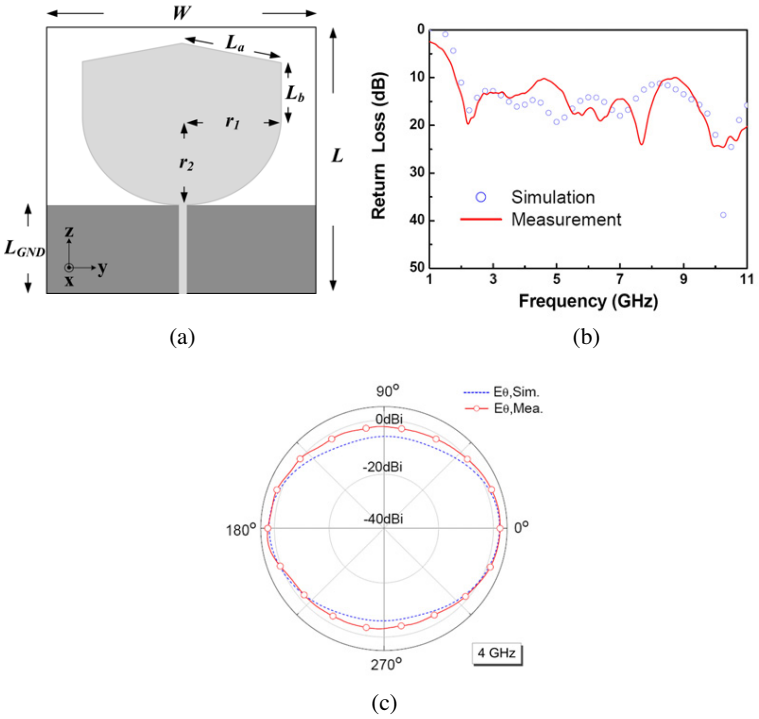

Figure 8. (a) Geometry, (b) return loss, and (c) xy-plane radiation pattern of the planar monopole antenna for transceiving ultrawideband signals.

to the shunt-mode pulse generator used in the transmitting module except that the frequency of the crystal oscillator is now 24.5536 MHz. By a multiplier factor of 12, the output clock rate is 294.6432 MHz. Unlike the transmitting module, however, here a pulse generator alone is adequate enough for generating LO strobes for sampling the received waveform. The strobe impulse converts into a pair of monocycle pulses with reverse polarity in the microwave sampler, as has been demonstrated in Fig. 5(b). The RF waveform received by the ultrawideband antenna is first divided into two branches by the T-junction of the sampler. It is then periodically sampled by the strobe impulses at the balanced sampling bridge. According to the equivalent time sampling theory [6], the equivalent sampling interval between two consecutive samples can be evaluated by

$$\Delta t = |1/f_{LO} - 1/f_{RF}| = 3.093\,\text{ps}. \tag{1}$$

In other words, if the pulse width of the RF signal is 500 ps, every single pulse reconstructed at the IF output will consist of more than 160 samples. Accordingly, the receiving module is capable of downsampling subnanosecond pulses with high accuracy. An active filter is connected to the output of the microwave sampler to filter out the high frequency components. The cutoff frequency is 12 MHz and the DC gain is 2.2. The downsampled pulse train has a pulse repetition frequency of 268.8 KHz, and is now ready for baseband processing.

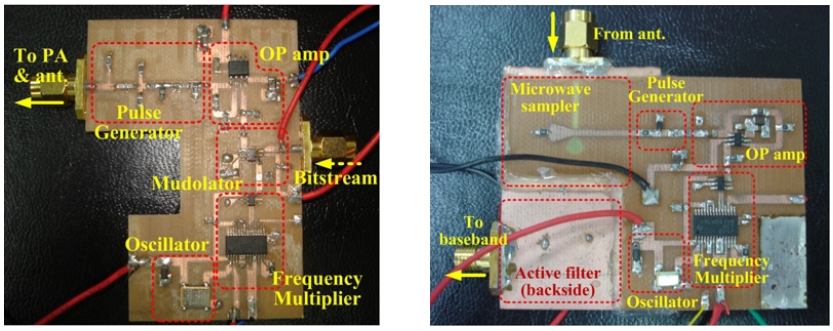

(a) (b)

Figure 9. Photographs of the fabricated (a) transmitting module and (b) receiving module.

Photographs of the fabricated transmitting and receiving modules are shown in Figs. 9(a) and (b), respectively. The antennas are not shown in the photographs for brevity. For demonstration in the laboratory, the power amplifier connected to the transmitter is an AR amplifier 1S1G4A with an 18-dB gain. The bitstream is generated by an Agilent 33220A arbitrary waveform generator. Two data rates, 90 Kbps and 270 Kbps, are demonstrated in the following discussions. Fig. 10(a) shows the modulated pulse train at the output of the pulse shaping network. The bit sequence has a repeated 1010 pattern with a data rate of 90 Kbps. Each bit actually consists of 3,277 (i.e., 294.912 MHz/90 KHz) RF pulses each with a peak amplitude of 0.3 V. Fig. 10(b) illustrates the individual RF pulses in a single bit. The RF pulse approximates to a second-order Gaussian derivative. The repetition frequency is 294.912 MHz and the pulse width is about 500 ps. To demonstrate sampled waveform in an ideal multipath-free environment, the transmitting and receiving modules were temporarily connected together by a coaxial cable. The power amplifier was temporarily removed as well. The waveform at the output of the microwave sampler is shown in Fig. 10(c). As shown in the figure, each bit consists of three downsampled second-derivative Gaussian

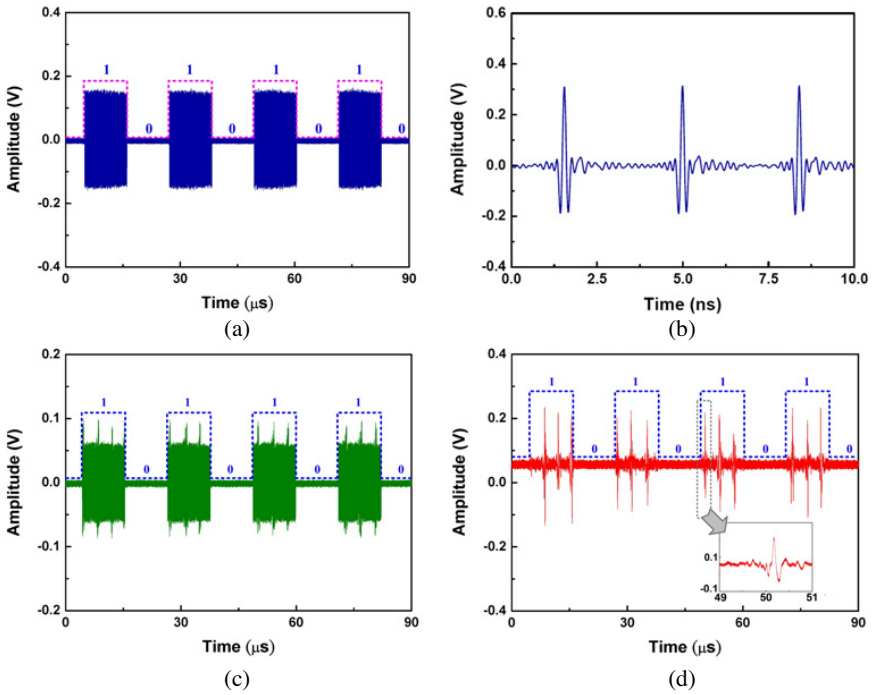

Figure 10. (a) Modulated pulse train at the output of the transmitting pulse generator. (b) Individual RF pulses in a single bit. (c) Sampled waveform at the IF port of the microwave sampler. (d) Output waveform at the filter output of the receiving module.

pulses since the 90-Kbps IF pulse train has a repetition frequency of 268.8 KHz. The filtered-out bitstream at the output of the lowpass filter is shown in Fig. 10(d). An enlargement of the downsampled pulse is shown in the inset as well. The output bitstream can be readily demodulated by a simple baseband processor. Additionally, it is worthwhile to mention that the filtered-out waveform has a 60-mV DC offset, which is likely a result of the noise power in the circuit.

Figure 11 shows experimental setup for validating the transceiving module over air interface. The experiment was completed in an anechoic chamber at National Taiwan University of Science and Technology. Two abovementioned ultrawideband antennas were mounted on the bakelite supporters to transmit and receive the modulated pulse train. The separation distance between the antennas was 2.3 m. The instruments including the power supply, oscilloscope, arbitrary waveform generator, and etc. were carefully shield by

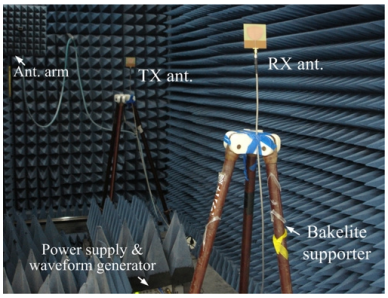

Figure 11. Experimental setup for demonstrating the proposed ultrawideband RF front-end module over air interface.

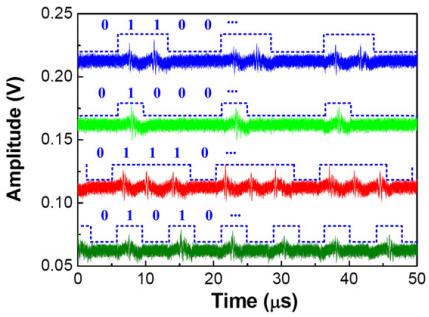

Figure 12. Sampled waveforms at the output of the receiving module for various bit patterns.

electromagnetic wave absorber to reduce multipath interference. The antenna arm in the background of the measurement setup, however, can be hardly shielded since the chamber is originally design for near-field measurement. Throughout the measurement the data rate is set to 270 Kbps, which in turn implies that each filtered-out bit contains only one downsampled pulse. Four repeated bit patterns, including 0101, 0111, 0001, and 0011, were fed into the transmitting module. The waveforms at the filter output are illustrated in Fig. 12. Due to the limited space, the waveforms are offset by 0, 50, 100, and 150 mV to facilitate the plot in the same figure. Referring to the figure, the outputs clearly demonstrate the desired bit patterns which can be readily demodulated by a baseband processor. Fig. 13 illustrates

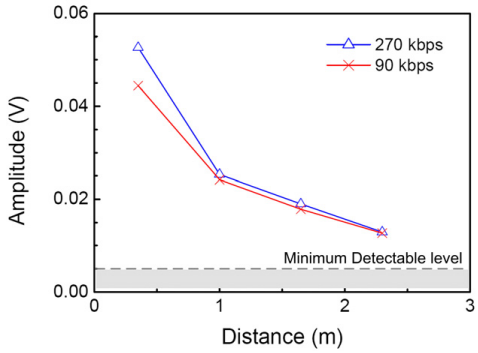

Figure 13. Received amplitude versus the separation distance between the transmitting and receiving antennas.

the received amplitude versus the separation distance between the transmitting and receiving antennas. Both data rates are evaluated at four different separations, i.e., 0.35, 1.0, 1.65, and 2.3 m. Referring to the figure, the output waveform roughly follows the $1/R$ fading. The maximum transmitting distance is estimated to be 4.5 m since the minimum detectable threshold is 5 mV above the average value of the bit streams, as has been illustrated in Fig. 12. Finally, it should be emphasized that further increasing the transmission data rate can be accomplished in two ways. Firstly, at the expense of a lower sampling accuracy, the data rate can be significantly improved by increasing the frequency difference between the RF and LO signals. For example, a transmission data rate of 2 Mbps is possible if the LO frequency is retuned to 292.912 MHz. However, the sampling points per reconstructed pulse drop dramatically from 160 to 21 points. Alternatively, if the frequencies of both LO and RF signals raise proportionally, the sampling accuracy can be retained while the data rate is effectively increased. For instance, the equivalent sampling interval is 8 ps if the LO and RF frequencies are set to 500 and 502 MHz, respectively. The resultant data rate will also be 2 Mbps but the sampling points per reconstructed pulse improve to 62 samples. The cost, nonetheless, rises accordingly since the clock generating circuit needs to be operated at a higher frequency.

5. CONCLUSION

An impulse-radio-based ultrawideband RF front-end module has been proposed and demonstrated in this paper. The proposed transceiving module is developed based on a novel multilayered microwave sampler. The microwave sampler is composed of a wideband multilayered magic-T and a balanced sampling bridge. The microwave sampler features high sampling accuracy with a compact size of 25 by 28 by 1.6 mm^3. By utilizing the equivalent time sampling theory and binary on-off keying modulation scheme, the proposed front-end module demonstrates a transmission data rate of 270 Kbps with coverage up to 4.5 m. The tradeoff for increasing the data rate has been discussed in this paper as well. The proposed RF front-end module may find applications in various circumstances such as in-vehicle communications, surveillance systems, and etc.. The future work will be in improving the dynamic range of the microwave sampler, reducing the power consumption of the front-end module, and in developing more complicated modulation scheme to further increase the data rate.

ACKNOWLEDGMENT

This work was supported by the National Science Council, R.O.C., under Grants 96-2221-E-011-007 and 97-2221-E-011-019-MY2.

REFERENCES

1. Aiello, G. R. and G. D. Rogerson, "Ultra-wideband wireless systems," *IEEE Microwave*, Vol. 4, No. 2, 36–47, June 2003.
2. Yang, L. and G. B. Giannakis, "Ultra-wideband communications: An idea whose time has come," *IEEE Signal Processing Magazine*, Vol. 21, No. 6, 26–54, Nov. 2004.
3. Fang, C., Y. Zheng, and C. L. Law, "An ultra wideband transmitter based on up conversion architecture," *Proc. IEEE Int. Workshop on Radio-frequency Integration Tech.*, 38–41, Singapore, Nov. 2005.
4. Ma, T. G. and C. F. Chou, "A compact multilayered magic-T in microstrip form and its application to microwave sampler," *2008 IEEE Int. Microw. Symp. Dig.*, 887–890, Atlanta GA, June 2008.
5. Remley, A. and D. F. Williams, "Sampling oscilloscope models and calibrations," *2003 IEEE Int. Microwave Symp. Dig.*, 1507–1510, Philadelphia, PA, July 2003.
6. Lawton, R., S. Riad, and J. Andrews, "Pulse & time-domain measurements," *Proc. IEEE*, Vol. 74, 77–81, Jan. 1986.
7. Madnani, K. and C. S. Aitchison, "A 20 GHz microwave sampler," *IEEE Trans. on Microw. Theory Tech.*, Vol. 40, No. 10, 1960–1963, Oct. 1992
8. Madani, K., "A hybrid 0.5–20 GHz microwave sampler," *IEE Colloquium on Multi-octave Microw. Circuits*, 3/1–3/4, London, UK, Nov. 1991.
9. Han, J. and C. Nguyen, "Coupled-slotline-hybrid sampling mixer integrated with step-recovery-diode pulse generator for UWB applications," *IEEE Trans. on Microw. Theory Tech.*, Vol. 53, No. 6, 1875–1882, June 2005.
10. Shamsinejad, S., M. Soleimani, and N. Komjani, "Novel enhanced and miniaturized 90° coupler for 3G EH mixers," *Progress In Electromagnetics Research Letters*, Vol. 3, 43–50, 2008.
11. Ohm, J. and M. Alberty, "Microwave phase detectors for PSK demodulators," *IEEE Trans. on Microw. Theory Tech.*, Vol. 29, No. 7, 724–731, July 1981.
12. Stec, B., C. Recko, and W. Susek, "Multibit microwave frequency

discriminators," *Proc. 2006 Int. Conference on Microw., Radar & Wireless Communications*, 240–242, May 2006.

13. Pozar, D. M., *Microwave Engineering*, 3rd edition, John Wiley & Sons, 2005.
14. Kim, J. P. and W. S. Park, "Novel configurations of planar multilayer magic-T using microstrip-slotline transitions," *IEEE Trans. Microw. Theory Tech.*, Vol. 50, No. 7, 1683–1688, 2002.
15. U-yen, K., E. J. Wollack, J. Papapolymerou, and J. Laskar, "A broadband planar magic-T using microstrip-slotline transitions," *IEEE Trans. Microw. Theory Tech.*, Vol. 56, No. 1, 172–177, Jan. 2008.
16. Fan, L., C.-H. Ho, S. Kanamaluru, and K. Chang, "Wide-band reduced uniplanar magic-T, hybrid-ring, and de Ronde's CPW-slot couplers," *IEEE Trans. Microw. Theory Tech.*, Vol. 43, No. 12, 2749–2758, Dec. 1995.
17. Gruszczynski, S., K. Wincza, and K. Sachse, "Design of compensated coupled-stripline 3-dB directional couplers, phase shifters and magic-Ts (Part II: Broadband coupled-line circuits)," *IEEE Trans. Microw Theory Tech.*, Vol. 54, No. 9, 3501–3507, Sept. 2006.
18. Wang, Z.-X., W. B. Dou, and Z.-L. Mei, "A compact H-plane magic tee designed at W band," *Progress In Electromagnetics Research B*, Vol. 5, 35–48, 2008.
19. Katsube, M. W., Y. M. M. Anter, A. Ittipiboon, and M. Cuhaci, "A novel aperture coupled microstrip magic-T," *IEEE Microw. Guided Wave Lett.*, Vol. 2, No. 6, 245–246, June 1992.
20. Davidovitz, M., "A compact planar magic-T junction with aperture-coupled difference port," *IEEE Microw. Guided Wave Lett.*, Vol. 7, No. 8, 217–218, Aug. 1997.
21. Fan, Z., L.-X. Ran, and J. A. Kong, "Source pulse optimizations for UWB radio systems," *Journal of Electromagnetic Waves and Applications*, Vol. 20, No. 11, 1535–1550, 2006.
22. Hall, R., S. Hamilton, and S. Krakauer, "Impulse-shunt made harmonic generation," *Proc. 1966 ISSCC*, 66–67, 1966.
23. Yin, X.-C., C.-L. Ruan, C.-Y. Ding, and J.-H. Chu, "A planar U type monopole antenna for UWB applications," *Progress In Electromagnetics Research Letters*, Vol. 2, 1–10, 2008.
24. Gopikrishna, M., D. D. Krishna, A. R. Chandran, and C. K. Aanandan, "Square monopole antenna for ultra wide band communication applications," *Journal of Electromagnetic Waves and Applications*, Vol. 21, No. 11, 1525–1537. 2007.